SAR SATELLITE IMAGE DERIVED WIND SPEED MAPS VALIDATED WITH IN-SITU METEOROLOGICAL OBSERVATIONS AND FOOTPRINT THEORY FOR OFFSHORE WIND RESOURCE MAPPING

Charlotte Bay Hasager*, Niels Otto Jensen*, Morten Nielsen*, Birgitte Furevik+
+Risø National Laboratory, Wind Energy Department,
DK-4000 Roskilde, Denmark, Phone +45 4677 5014 / Fax +45 4677 5970
*Nansen Environmental and Remote Sensing Center
Edvard Griegsvei 3A, N-5059 Bergen, Norway. Phone +47 55297288, Fax +47 5520 0050

ABSTRACT: Synthetic Aperture Radar (SAR) satellite images from the European satellite ERS-2 are used for deriving wind speeds and wind directions offshore for 16 cases in the North Sea. The area investigated is the Horns Rev site 15 km west of the Jutland coast in Denmark. It is investigated how well satellite SAR wind speed maps correspond to in-situ mast observations. The SAR satellite wind speed mapping is performed with an empirical algorithm (CMOD-IFR2). The physical principle is based on the near-instantaneous wind interaction at the sea surface generating capillary and short gravity waves. The pattern of these waves is related to the radar backscatter signals received by the satellite. The resolution of the maps is 400 by 400 m covering 100 by 100 km as snapshots (within a few seconds) around every third day. A simple footprint method is used as a tool to compare spatial (SAR) and temporal (meteorological) data. The footprint theory takes into account the relative influence of the upwind conditions to the observed wind speed as a function of measurement height and stability. The results are promising with high correlation between in-situ and SAR wind speed and SAR wind direction.

1 INTRODUCTION

Offshore wind resources are of major interest for the siting of offshore wind farms. A quick and simple method for offshore wind resource estimation may be offered by satellite image wind speed mapping in the early planning phase. The satellite observations are readily available from satellite archives so it is not necessary to wait for a one-year time-series to be collected. The SAR wind speed technology is new. A validation study as well as the development of a useful tool is carried out in an ongoing EU research project called WEMSAR, acronym for Wind Energy Mapping using SAR. SAR is Synthetic Aperture Radar.

The current paper describes the SAR observations, the method of calculating the SAR images into wind speed maps and the possible errors associated including collocation. Further is described the validation of SAR wind speed maps to in-situ meteorological observations from a site in the North Sea. Footprint area-averaging is used for the comparison of the spatial satellite observations to time-series mast observations. A discussion on the results and recommendation for practical use of SAR wind speed maps is given in the end of the paper.

2 SYNTHETIC APERTURE RADAR (SAR)

2.1 Satellite image availability

The satellite images that have proven useful for wind speed mapping over the ocean are the C-band SAR. These images are available from 4 different satellites and the historical SAR image archive dates back to July 1991. The orbits of all four satellites are so-called sun-synchronous, i.e. each area of the globe is image at approximately the same local time in a repeat cycle of a few days. The satellite and sensors are listed in Table I. The ERS and ENVISAT satellites are owned by the European Space Agency (ESA). The images are available for research and application through Announcements of Opportunity (AO) but also for operational and commercial use. The price of ENVISAT is expected to be at or near the cost of reproduction (1). RADARSAT is owned by the Canadian Space Agency and are more expensive at the moment.

Table I List of available satellite SAR images in C-band with vertical (VV) and horizontal (HH) polarizations.

Satellite/ instrument	Period	
ERS-1 SAR	Jul.91-Jun.96	C-VV
ERS-2 SAR	April 1995-	C-VV
RADARSAT-1	Nov. 1995-	C-HH
ENVISAT ASAR	March 2002-	C-VV, HH

ERS-2 SAR images have been analysed in the current study. From ERS-2 SAR there is about 36 images available per year for a given site i.e. provided the images were downloaded by a receiving station and archived. Some remote parts of the globe may not be (fully) covered. For information on the availability for a specific site please visit ESA's web page http://odisseo.esrin.esa.it/ at which the archive is located. ERS SAR quicklook images exist for some cases. The quicklook images are free of cost and useful for a quick evaluation of the data quality (including certain atmospheric and marine features). However, only by analysing SAR raw data can the wind speed maps be calculated

2.2 SAR signals

The principle of the ERS SAR system is sketched in Fig. 1. The SAR emits C-band microwave radiation in an angle to the side of the flight direction. The radar beam reaches the Earth with an incidence angle (γ) between 20 and 26º in the cross track direction. The width of the cross track is the swath which is 100 km. The microwave signal is backscattered in all directions at the surface. Those signals that happen to travel back to the SAR are measured. As the satellite moves along track the Earth is imaged continously. A two-dimensional data set (image) is obtained through a calculation of the time delay between emitted and received radiation, the slant range,

ground range and azimuth geometry. The cell size of raw data is 26 m in range (antenna look direction) and between 6 and 30 m in azimuth (in-flight direction) (2). A SAR image is 100 km by 100 km. SAR has a 24-hour recording capability independent of daylight and SAR is penetrating cloud and rain.

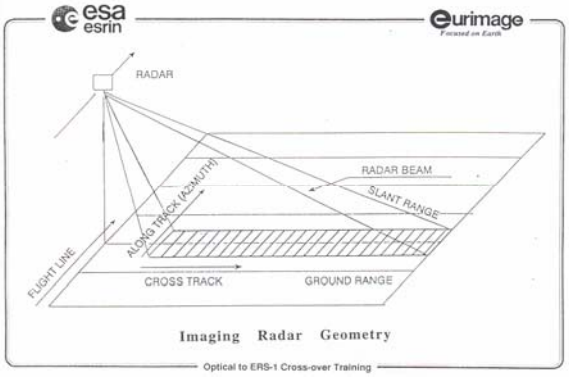

Fig. 1 Principle of ERS SAR scanning system. From (3)**.**

2.3 Wind speed from SAR

The ERS SAR C-band has a wavelength of 5.3 cm. SAR signals that reach the ocean surface is backscattered as a function of the gravity-capillary surface waves generated by the local wind field. At the ERS SAR incidence angles, the radar backscatter, or more precisely, the normalized radar cross section, σ_0, is dominated by Bragg scattering from cm-scale ocean surface roughness, which is in resonance with the incidence radiation of the radar. The larger the wind speed, the rougher is the surface and hence the greater is the backscatter. A very smooth surface will appear as black in a SAR image.

Described in more detail the amplitude of gravity-capillary waves saturate for the wind condition of a few meters per second. At increased wind speeds the momentum flux is continously carried into the air-sea interface and causes underlying longer-wavelength surface waves to increase in amplitude on a scale greater than or equal to tens of seconds. Such an increase induces tilting in the gravity-capillary wave field, which makes the ocean surface more visible (brighter) to radar. This accounts for the general increase in radar backscatter with mean wind speed (u) (4).

Φ^0 measured in each resolution cell is a function of $\forall$, u and the angle between wind direction and range (N). Theoretical studies of the relationship between Φ^0 and N for C-band VV (5) show a symmetrical response with minimum errros on crosswind, upwind and downwind cases and maximum errors on winds at angles of ±45º and the error increases for higher wind speeds. Therefore the angle between wind direction and range has to be known **a priori** for the wind speed to be retrieved accurately from a SAR image.

In most cases the wind direction may be determined from streaks, i.e. visible linear features in the SAR images. The accuracy of SAR streak direction compared to in-situ wind observations show some scatter e.g. up to 30º (6). Otherwise an estimate of wind direction from a meteorological model or in-situ observations will have to be used.

SAR wind speed retrival algorithms are based on C-band scatterometer algorithms e.g. CMOD-4 (7) and CMOD-IFR2 (8). The latter is used in the current study. The wind speed is calculated for a height of 10 m above sea level.

2.4 Errors on SAR wind speed

The radiometric accuracy of ERS-1 and –2 SARs is within ±0.4 dB (1) that translate to approximately ± 0.7 m s^{-1}. This accuracy is much smaller than the overall accuracy of the wind speed models where the wind speed is solved within 2 m s^{-1} or 10 % in rms for wind speeds between 2 - 24 m s^{-1} (7). Some studies have shown the accuracy in ERS SAR to be better e.g. 1.2 to 1.5 m s^{-1} in some cases (9) and (10). The method of comparison between SAR wind speed maps and in-situ observations is of importance. A significant amount of error may be due to poor collocation in space and in time. Other errors relate to oceanic, atmospheric and speckle noise.

Speckle noise is due to scattering of coherent electromagnetic waves by rough surfaces. Multi-looking, i.e. averaging a number of cells, reduces the speckle noise but also reduces the spatial resolution. Speckle noise is dominating for 100-400 m pixels. For very large grid cells (e.g. 10 km) speckle noise is reduced to an insignificant level in ERS SAR (5).

Atmospheric noise may stem from rain volume scattering that reduce σ_0. Oceanic noise may stem from surfactants (e.g. oil slicks, algal blooms) at the ocean surface. Surfactants are very effective at damping the wind generation of Bragg waves, hence under moderate winds surfactants can be delineated in SAR imagery. However for winds > 5 m s^{-1} the surface layer tends to mix down into the water column and become undetectable by SAR (11). Finally should shallow water and tidal currents be mentioned as possible sources of error in wind speed estimation from SAR.

2.5 Collocation

The issue of collocation is that of precise geolocation and timing. Collocation is fundamental to wind speed retrieval from SAR. Problems related to collocation influence the CMOD scatterometer algorithms themselves as well as the independent SAR wind speed validation studies.

CMOD-IFR2 is based upon wind speed data from 3433 collocated pairs of buoy data, ECMWF (European Center of Medium-range Weather Forecast) model results and scatterometer data. Buoy observations are too sparse to cover the global oceans, hence it is an advantage to use ECMWF model results in the correlations. Atmospheric model results may however not capture all atmospheric events equally well. Scatterometer data typically has a resolution of 25 by 25 km or 50 by 50 km grid cells. The correlation analysis between so large grid cells and buoy data can suffer from smaller scale gradients within the cells that are averaged out. Further does buoy wind speed observations suffer an overestimation of low winds and overestimation of medium and high winds. Above 25 m s^{-1} the buoys fail to respond. The problems are due to tilting and displacement height in high seas (12).

Buoys may shift significantly from their nominal position around 1 km for deep ocean (13) and the geometrical rectification of satellite scenes from the open ocean may

be rather poor because it only can be done from the nominal coordinates due to a lack of ground control points. In other words the collocation in space may be inaccurate.

In coastal regions geometrical rectification with ground control points from islands and coasts typically give a much better geolocation (subgrid accuracy). For independent validation studies on SAR wind speed maps the comparison may be made to in-situ data from buoys, ships or mast, either coastal or offshore. Meteorological masts have the advantage of well-known positions, hence only the geometrical correction of satellite images can introduce a small error in collocation in space. The position of ships is probably better known than ocean buoys, yet less accurate than a mast. According to (14) available ship wind speed observations are of a poor quality compared to buoys, except for some research vessels when these meteorological data are properly processed. For coastal masts the effect of the land surface orography (topography), even very modest orography, will influence the observations as compared to the wind speed over the ocean. A method for the correction of land surface orography is described in detail in (15). Offshore masts are the ideal choice for validation studies.

Collocation in time deals with the issue of comparing spatial data to time samples. SAR wind speed maps are spatial snap-shots within seconds. Meteorological observations are time-averaged data from single points. Taylor's hypothesis on frozen turbulence is used extensively to describe spatial atmospheric phenomena based on meteorological point observations (16). In a number of independent SAR wind speed validation studies the spatial and temporal scale have been considered in different ways. The methods are listed below. (17) cropped a SAR wind speed map into square sub-scenes of the size order of 20-50 km^2 for comparing to 8-minute buoy observations.(18) chose a 3 by 3 km area centered on the buoy location when comparing buoy data to SAR wind speeds. Katsaros et al. cited in (19) used a 64 km^2 area for comparison and (10) used a 4 km^2 area for ship comparison.

In the current study high-quality mast data from Horns Rev in the North Sea (20) are used for an independent SAR wind speed validation study and the area-averages from the SAR wind speed maps are calculated from footprint theory.

3 FOOTPRINT THEORY

The theory on scalar footprints originates from (21). The concept is that air is advected to a sensor at a given height from the upwind source area graphed in Figure 2. In the area close to the sensor there is a large amount of influence whereas the area further away has less influence. The footprint area-averaging method has mainly been used for land surfaces but an example by (22) shows the use of footprint theory also in a marine study.

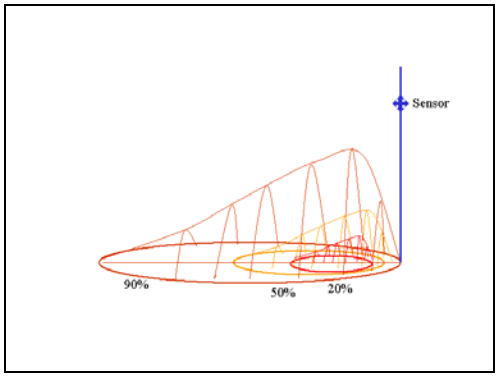

Figure 2 Schematic of the footprints for a given sensor. The area giving a certain percentage of influence to the signal is shown for 20 %, 50 % and 90 %.

(21) proposed a crosswind-integrated footprint of the type

$$f^{y}(x) = \frac{A}{x^2}\exp\left\{-\frac{A}{x}\right\}, \quad \text{for } x > 0$$

The length scale $A=uz_m/\kappa u_*$ depends on a uniform advection velocity (u), the flux measurement height (z_m), and the friction velocity (u_*), κ is the von Karmán constant. The footprint was derived under the assumption that the vertical profile of a plume from a ground source has an exponential shape and the advection speed is considered uniform. The x-axis is in the upwind direction and the integral from the mast position to infinity is unity. The maximum is found at the distance $x=A/2$ and the downwind footprint integral is

$$F^{y}(x) = \exp\left\{-\frac{A}{x}\right\}, \quad \text{for } x > 0$$

(23) and (24) extended the theory to include corrections for static stability. All models have been tested. The pixel-area integrals are calculated as follows.

The satellite image is described in the UTM system with X (East) and Y (North) in metres and the mast position is (X_m, Y_m). The wind direction χ is measured anticlockwise from North, see Figure 3, and the transformation to footprint coordinates is:

$$\begin{bmatrix} x \\ y \end{bmatrix} = \begin{bmatrix} \sin\theta & \cos\theta \\ -\cos\theta & \sin\theta \end{bmatrix} \cdot \begin{bmatrix} X - X_m \\ Y - Y_m \end{bmatrix} \Leftrightarrow$$

$$\begin{bmatrix} X \\ Y \end{bmatrix} = \begin{bmatrix} X_m \\ Y_m \end{bmatrix} + \begin{bmatrix} \sin\theta & -\cos\theta \\ \cos\theta & \sin\theta \end{bmatrix} \cdot \begin{bmatrix} x \\ y \end{bmatrix}$$

The footprint in image resolution is estimated by a set of observation points distributed evenly over the footprint area. This is done by the reverse functions of the accumulated downwind and lateral distributions and the observation point is translated to image coordimates. With a large number of observation points, e.g. 1000×1000, the particle count becomes a reliable estimate of the relative weight of individual pixels.

for $i = 1 \ldots N_x$ do
begin
$x = \mathrm{F}^{-1}\left[\left(i - \frac{1}{2}\right)/N_x\right]$
for $j = 1 \ldots N_y$ do
begin
$y = \sigma(x_i) \cdot \Phi^{-1}\left[\left(j - \frac{1}{2}\right)/N_y\right]$
$(x, y) \rightarrow (X, Y)$
end
end

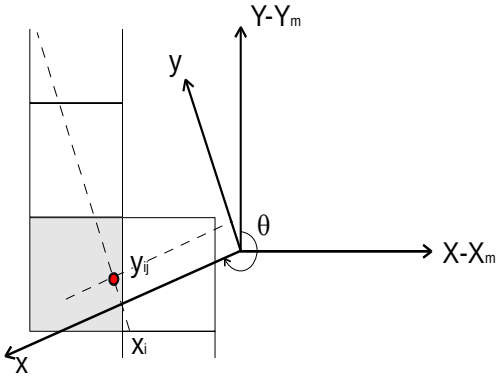

Figure 3 Sketch of the geometry of pixel-area integration

4 VALIDATION RESULTS

Validation results of comparing in-situ meteorological mast observations and SAR satellite wind speed maps by use of footprint theory are shown in Table II and

Table II SAR wind speed values at Horns Rev from in-situ mast data, simple and advanced footprint from SAR wind speed maps. * proxy values from a box.

	Date	In-situ	Simple footprint Mean	Simple footprint Std. dev.	Advanced footprint Mean
		(m s^{-1})	(m s^{-1})	(m s^{-1})	(m s^{-1})
1	19990520	7.8	1.7	0.41	1.8
2	19990621	10.1	9.0	0.85	9.6
3	19990710	4.2	1.8	0.43	1.8
4	19990729	5.6	5.2	0.56	5.8
5	19990810	11.2	8.8	0.41	8.8
6	19990830	7.0	6.3	1.1	6.9
7	19991003	11.9	11.5	0.95	9.2
8	19991007	10.4	9.4	0.34	10.4
9	19991019	8.9	8.4	0.53	9.9
10	19991123	1.6	0.5	0.21	0.8
11	19991216	9.9	9.5	0.30	9.5
12	20000116*	7.7	6.8	0.54	8.5
13	20000201	10.5	9.7	0.46	9.8
14	20000307	12.2	11.4	0.35	11.9
15	20000326*	4.3	2.0	0.82	2.8
16	20000516	4.8	0.4	0.27	0.1

The simple footprint is an ellipse with a major and a minor axis of 5.5 km and 1.0 km, respectively, i.e. a total of 26 pixels that are weighted equally. The advanced footprints are calculated as described in section 3. For two cases (#12 & 15) the SAR wind speed maps did not contain the true footprint areas, therefore a box-average in the vicinity is used as a proxy.

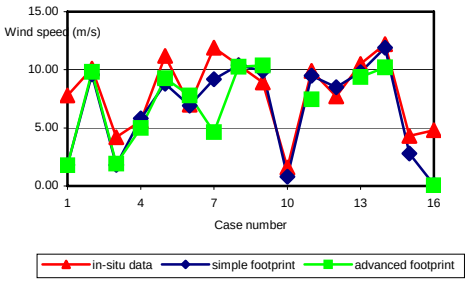

Figure 4 SAR wind speed values at Horns Rev from in-situ mast data, simple and advanced footprint from SAR wind speed maps.

Linear correlation results between the in-situ observations and footprints are calculated and listed in Table III. A higher correlation is found for the simple footprints (R^2=0.77) than the advanced footprint (R^2=0.50). Within each simple footprint the standard deviations are listed in Table II for the wind speed maps based on SAR wind streak direction. The standard error is 0.53 m s^{-1} on average for the simple footprints.

SAR wind speed maps derived using in-situ wind direction (instead of SAR streak direction) are also calculated. Linear correlation results of simple footprints from those maps and in-situ data are given in Table III (R^2=0.8). This correlation is the best. The standard error is 0.61 m s^{-1} but the bias (-2.3 m s^{-1}) is larger than for SAR wind speed maps based on SAR streak direction.

Table III Linear correlation results for in-situ mast observations and SAR wind speed maps with input of wind direction from SAR wind streaks. * wind direction from in-situ observations.

Simple footprint	y=1.1016x-2.1263	R^2=0.77
Advanced footprint	y=0.9681x-1.7626	R^2=0.50
Simple footprint*	y=1.0436x-2.2767	R^2=0.81

The in-situ wind direction and SAR streak directions are compared and the linear correlation is y = 1.1113x - 31.576 with R^2 = 0.9487 so the correlation is high, yet there is a bias of 31°.

5 DISCUSSION AND RECOMMENDATIONS

The satellite SAR-derived wind speed maps can map the actual wind speed as a snapshot in time with a standard error around 0.61 m s^{-1}. Speckle error inherent in SAR wind speed maps relating to spatial resolution (here 400 by 400 m pixels) may be the explanation for the better correlation of the simple averaging than the advanced footprints. The advanced footprints are more correct from a physical point of view but in this footprint averaging a single pixel is given between 10-75% weight which may introduce error that is avoided when 26 pixels in the simple footprint are weighted equally.
SAR wind speed maps derived from in-situ wind direction give a better estimate than those derived from SAR streak direction (R2 is higher but the bias is also higher). (10) also found the in-situ observations (from a

ship) to improve wind speed maps compared to SAR streak directions. However in most practical cases only SAR streaks or meteorological model results will be available for the SAR algorithm.

An analysis of SAR streak accuracy and the angle between wind direction and range could be useful for further analysis as well as a larger number of SAR scenes. Multilooking the SAR data further could reduce speckle noise. The trade-off between spatial resolution and speckle noise could be analysed further. Alternatively could high-resolution SAR wind speed maps be filtered prior to calculating footprint averages.

Around 100-300 satellite SAR images are available for some sites on Earth since 1991 but far fewer (or none) in certain areas. New scenes can be ordered and taken from a site if needed. Under the assumption that there are no errors in SAR wind speed maps (25)) demonstrate that 60-70 images can estimate the mean wind speed and Weibull c parameter while 150 images are required to obtain a variance estimate within ±10% at a 90% confidence level.

For wind resource calculation the advantages of SAR wind speed maps are that they are readily available and they can show gradients over rather short distances, i.e. variations in the windpower potential.

6 ACKNOWLEDGEMENTS

Funding for WEMSAR contract ERK6-CT-1999-00017, ERS SAR satellite images from ESA AO3-153 and meteorological data from Horns Rev from Techwise are much appreciated. Ebba Dellwik calculated the 10 m in-situ wind speeds from the profile data.

REFERENCES

[1] E.Attema, Y.-L.Desnos, and G.Duchossiois, Synthetic aperture Radar in Europe: ERS, Envisat, and beyond, John Hopkins APL Technical Digest 21:155 (2000).
[2] J.Horstmann, W.Koch, S.Lehner, and R.Tonboe, Wind retrieval over the ocean using synthetic aperture radar with C-band HH polarization, IEEE Transactions on Geoscience and Remote Sensing 38:2122 (2000).
[3] ESA. Optical to ERS-1 SAR: A cross-over course at ESRIN. 1993. Ref Type: Report
[4] P.D.Mourad, D.R.Thompson, and D.C.Vandemark, Extracting fine-scale wind fields from synthetic aperture radar images of the ocean surface, John Hopkins APL Technical Digest 21:108 (2000).
[5] J.Horstmann, S.Lehner, W.Koch, and R.Tonboe, Computation of wind vectors over the ocean using spaceborne syntheric aperture radar, John Hopkins APL Technical Digest 21:100 (2000).
[6] P.W.Vachon and E.W.Dobsen, Wind retrieval from RADARSAT SAR images: selection of a suitable C-band HH polarization wind retrieval model, Canadian Journal of Remote Sensing 26:306 (2000).
[7] A.Stoffelen and A.D.L.T., Wind retrieval and ERS-1 scatterometer radar backscatter measurements, Advance Space Research 13:53 (1993).
[8] Y.Quilfen, B.Chapron, T.Elfouhaily, K.Katsaros, J.Tournadre, and B.Chapron, Observation of tropical cyclones by high-resolution scatterometry, Journal of Geophysical Research 103:7767 (1998).
[9] D.Offiler, The calibration of ERS-1 satellite scatterometer winds, Journal of Atmospheric and Oceanic Technology 11:1002 (1994).
[10] P.W.Vachon and F.W.Dobson, Validation of wind vector retrieval from ERS-1 SAR images over the ocean, Global Atmosphere and Ocean System 5:177 (1996).
[11] P.Clemente-Colón and X.-H.Yan, Low-backscatter ocean features in synthertic aperture radar imagery, John Hopkins APL Technical Digest 21:116 (2000).
[12] R.A.Brown, On satellite scatterometer model functions, J. Geophysical Research 105:29195 (2000).
[13]J.S.S.Gower, Wind, slick, and fish boat observations with Radarsat ScanSAR, John Hopkins APL Technical Digest 21:68 (2000).
[14] R.Atlas, R.N.Hoffman, S.M.Leidner, J.Sienkiewicz, T.-W.Yu, S.C..Bloom, E.Brin, J.Ardizzone, J.Terry, D.Bungato, and J.C.Jusem, The effects of marine winds from scatterometer data on weather analysis and forecasting, Bulletin of the American Meteorological Society 82:1965 (2001).
[15] C.B.Hasager, F.H.P., and B.R.Furevik, On offshore wind energy mapping using satellite SAR, Canadian Journal of Remote Sensing 28:x (2002).
[16] R.B.Stull, "An introduction to boundary layer meteorology", Kluwer Academic Pub., Dordrecht (1991).
[17] T.D.Sikora and D.R.B.J.C.Thompson, Testing the diagnosis of marine atmospheric boundary-layer structure from synthetic aperture radar, John Hopkins APL Technical Digest 21:94 (2002).
[18] F.M.Monaldo, D.R.Thompson, R.C.Beal, W.G.Pichel, and P.Clemente-Colón, Comparison of SAR-derived wind speed with model predictions and ocean byou measurements, IEEE Transactions on Geoscience and Remote Sensing (2001).
[19] P.D.Mourad, Footprints of atmospheric phenomena in synthetic aperture radar images of the ocean surface: a review, *in:* "Air-SEa Exchange: Physics, Chemistry and Dynamics", G.L.Geernaert, ed., Kluwer Academic Publishers, Dordrecht (1999).
[20] S.Neckelmann, J.Petersen. Evaluation of the stand-alone wind and wave measurement systems for Horns REv 150KW offshore wind farm in Denmark. 2000. Rome, ATENA/ENEA. Proceedings of OWEMES offshore wind energy in Meidterranean and other European Seas, 13-15 April 2000, Sircusa, Sicily, Italy.
[21] J.H.C.Gash, A note on estimating the effect of a limited fetch on micrometeorological evaporation measurements, Boundary-Layer Meteorology 35:409 (1986).
[22] A.Smedman, U.Hogstrom, H.Bergstrom, A.Rutgersson, K.K.Kahma, and H.Pettersson, A case study of air-sea interaction during swell conditions, J. Geophysical Research-Oceans 104:25833 (1999).
[23] C.H.Hsieh, C.Katul, and T.W.Chi, An approximate analytical model for footprint estimation of scalar fluxes in thermally statified atmospheric flows, Advanced Water Research 23:765 (2000).
[24] T.W.Horst and J.C.Weil, How far is far enough? - The fetch requirements for micrometeorological measurement of surface fluxes, Journal of Atmospheric and Oceanic Technology 11:1018 (1994).
[25] S.P.Pryor, R.J.Barthelmie, and C.B.Hasager, Can satellite sampling of offshore wind speeds represent wind speed distributions?, Global Windpower, this issue (2002).